

Synchrony and Entrainment Properties of Robust Circadian Oscillators

Neda Bagheri^{*1}, Stephanie R. Taylor^{†1}, Kirsten Meeker[‡],
Linda R. Petzold[§], Francis J. Doyle III^{¶2}

^{*}Department of Electrical and Computer Engineering,
University of California, Santa Barbara, CA 93106-9560;
Email: neda@ece.ucsb.edu

[†]Department of Computer Science,
University of California, Santa Barbara, CA 93106-5110;
Email: staylor@cs.ucsb.edu

[‡]Department of Computer Science,
University of California, Santa Barbara, CA 93106-5110;
Email: kmeeker@cs.ucsb.edu

[§]Department of Computer Science,
University of California, Santa Barbara, CA 93106-5110;
Email: petzold@cs.ucsb.edu

[¶]Department of Chemical Engineering,
University of California, Santa Barbara, CA 93106-5080,
Department of Biomolecular Sciences and Engineering,
University of California, Santa Barbara, CA 93106-9611;
Email: doyle@engineering.ucsb.edu

Abstract

Systems theoretic tools (i.e. mathematical modeling, control, and feedback design) advance the understanding of robust performance in complex biological networks. We highlight internal time (or *phase*) as a key performance measure used to investigate dynamics of a single deterministic circadian oscillator for the purpose of generating insight into the behavior of a population of oscillators. More specifically, such analysis identifies appropriate coupling mechanisms for the ensemble of noisy (stochastic) circadian clocks. Phase also serves as a critical control objective to correct mismatch between the biological clock and its environment.

Keywords: Circadian clocks, phase response curves, coupled oscillators, control, stochastic simulations.

¹N.B. and S.R.T. contributed equally to this work.

²Corresponding author: frank.doyle@icb.ucsb.edu.

1 Introduction

Undergirding a biological system are networks of interacting components. To elucidate the mechanisms employed by these networks, biological experimentation and intuition are by themselves insufficient [1]. In the field of systems biology, investigators characterize dynamics via mathematical models and apply systems theory with the goal of guiding further experimentation to better understand the biological network that gives rise to robust performance [2]. An ideal example of biological complexity is the circadian clock, which coordinates daily physiological behaviors of most organisms.

The mammalian circadian master clock resides in the suprachiasmatic nucleus (SCN), located in the hypothalamus [3]. It is a network of multiple autonomous noisy oscillators, which communicate via neuropeptides to synchronize and form a coherent oscillator [4, 5]. This coherent oscillator then coordinates the timing of daily behaviors, such as the sleep/wake cycle. Left in constant conditions, the clock will free-run with a period of only *approximately* 24 hours such that its internal time, or *phase*, drifts away from that of its environment. Thus, vital to a circadian clock is its ability to entrain to external time through environmental factors [6–8]. To study the timekeeping of circadian clocks, we employ systems theory to analyze two complementary cases: one involving the network of coupled oscillators, and the other involving the single coherent oscillator. In both cases the measure of performance relates to the system’s phase response behavior. A phase response curve (PRC) characterizes the clock’s time-dependent sensitivity to a given stimulus (in this work, a pulse of light or a neuropeptide). A clock adjusts its phase according to the time of day the stimulus is perceived. Thus, the PRC maps the signal’s arrival time to the resulting phase shift (an advance or delay) [8].

To further our understanding of synchronization and entrainment, we use ordinary differential equations (ODEs), stochastic differential equations (SDEs), and a discrete stochastic model in both the network and single-cell setting. Circadian clocks modeled as single, deterministic ODE limit cycle oscillators [9, 10] are used to study both the internal composition of the clock and the process of entrainment by light/dark cycles [11]. To capture the variability observed in biological data, additional models introduce stochasticity via multiplicative noise in SDEs [12], or via an extension of the model from differential to discrete stochastic equations [13]. To capture network behavior, spontaneous synchronization of coupled oscillators is modeled for the mammal and fly [12, 14, 15]. In Section 2, we simulate a population of mammalian neurons using a discrete stochastic model. The challenges associated with achieving synchronization are addressed via the study of a single oscillator. In Section 3, we simulate an SDE model and analyze the period of the synchronized neurons by studying the phase response

behavior of a single, deterministic cell. Section 4 describes a strategy that makes use of the light-induced circadian phase response to correct phase mismatch that arises when there is a difference between internal and external time.

2 Modeling Coupled Stochastic Mammalian Neurons

Biological experiments show that uncoupled neurons in the SCN are either damped or sloppy oscillators [16]. These neurons are synchronized daily via vasoactive intestinal (neuro)peptide (VIP) [4], whose intercellular concentration levels peak during the subjective day. Preliminary results demonstrate that controlled VIP pulses cause phase shifts similar to those resulting from light pulses, suggesting that the VIP signal and target are similar to those of light and may be modeled correspondingly. The target of VIP signaling is therefore assumed to be *per* transcription [17].

Experimental data demonstrates that isolated (uncoupled) neurons exhibit both a broad distribution of periods and temporal (cycle-to-cycle) variability [4]. Hao *et al.* [18] and To *et al.* [15] postulated mechanisms through which VIP signals are received by a cell via signal cascades culminating in the modulation of the parameter associated with *per* transcription. Using an ODE model, To *et al.* incorporate this coupling mechanism into a population of non-identical cells, each of which is based on the gene regulatory network model of Leloup and Goldbeter [10]. They simulate scenarios with no coupling (the cells drift out of phase), and with coupling (the cells form a coherent oscillator), demonstrating that their mechanism is capable of creating the spontaneous synchronization seen in experimental data. Likewise, their simulations show a broad distribution of periods across cells. However, because they use a deterministic model, they do not reproduce cycle-to-cycle variation. We develop a discrete stochastic model based on that in [15] incorporating intrinsic noise, and consequently temporal variability.³ We simulate this model in a 2-dimensional grid of 9 SCN neurons using a software package [20] based on the Stochastic Simulation Algorithm (SSA) [21, 22]. Successful synchronization of 9 coupled cells validates the mechanism in the presence of noise.

³Gillespie offers an explanation of the conditions under which Langevin and deterministic chemical kinetics approximations are valid [19]. This is usually the case when populations of all the reactant species are sufficiently large. This may not be true in the biological system being modeled, and is not the case in the predictions of the Leloup and Goldbeter deterministic model (some species concentrations approach zero during low points in the oscillatory cycle), so a deterministic approximation using ODEs may not be adequate for our purposes.

2.1 Simulating a Single Cell

The introduction of noise alters the behavior of the single cells such that additional tuning is required to achieve synchrony. In particular, because VIP signaling ultimately manifests as modulation of the rate of *per* transcription, special attention must be paid to the levels of *per* mRNA and its rate of transcription, $\nu_{sP}(t)$. The basal rate, ν_{sP0} , characterizes the behavior of an isolated cell: *per* mRNA oscillations are damped when $\nu_{sP0} < 1.2$, sustained when $1.2 \leq \nu_{sP0} \leq 1.8$, and unrealistically high in amplitude (and minima) when $\nu_{sP0} > 1.8$ (see Fig. 1). The depletion or accumulation of *per* mRNA that occurs when ν_{sP0} is below 1.2 or above 1.8 indicates that the balance is upset between the transcription rate and the combination of the transport (from nucleus to cytoplasm) and degradation. For the coupled population to exhibit synchrony, we have observed that the median value of $\nu_{sP}(t)$ must stay within the range that produces oscillations in an individual cell. Thus, to achieve synchrony, the basal transcription rate ν_{sP0} has been decreased to 1.0 for the coupling grid size and weight used in the present work. To maintain control of the median *per* mRNA population, we simulate with only a small amount of intrinsic noise. In the SSA, this is done by increasing the volume of the simulation (thus increasing the number of molecules and the signal to noise ratio). We are able to produce a median *per* mRNA population comparable to the uncoupled case with $\nu_{sP0} = 1.5$. At this basal transcription rate, all isolated cells are damped oscillators. To better match the biological observation that many isolated cells show sustained oscillations, it is necessary to either weaken the coupling, or adjust the transport or degradation rate to re-balance the *per* mRNA level.

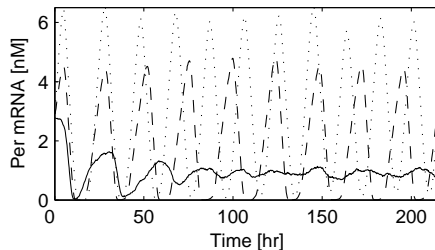


Figure 1: *Per* mRNA concentration as a function of basal transcription rate ν_{sP0} in uncoupled cells. The solid line represents a simulation where $\nu_{sP0} = 1$, the dashed line $\nu_{sP0} = 1.5$, and the dotted line $\nu_{sP0} = 2$. For ν_{sP0} below 1.2, *per* mRNA concentrations exhibit damped oscillations for the ten day period simulated. For ν_{sP0} above 1.8, *per* mRNA concentrations begin to grow in amplitude with minima greater than zero.

2.2 Simulating a Population

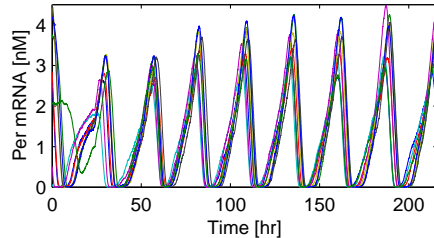
Simulation of a 3×3 grid of cells (with coupling enabled at 24 hours) shows that the mechanism is capable of achieving synchrony (Fig. 2). To measure the phase coherence of the cells in a simulation, we use the radius $r(t)$ of the complex order parameter [23], computed according to

$$r(t) = \frac{1}{N} \sum_{j=1}^N e^{i(\theta_j - \Psi)},$$

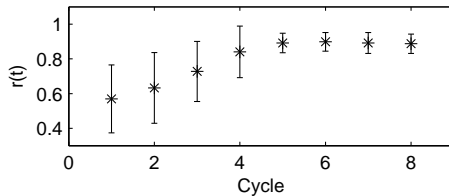
where N is the number of cells, θ_j is the phase of the j^{th} oscillator, and $\Psi(t)$ is the average phase. If the oscillators are in phase, $r(t) \approx 1$. Here, the mean $r(t)$ across 25 simulations begins at 0.56 when the system is uncoupled, and increases from 0.63 to 0.84 in two cycles when coupled. As the system transitions from asynchrony to synchrony, the standard deviation of $r(t)$ decreases, showing that coupling decreases the effects of noise over time. Together, these data demonstrate the quick and effective response of intercellular signaling that gives rise to phase synchrony. However, we do not capture the desired period and temporal variability (data not shown). This will require increasing the effective noise level by lowering the volume, with possible further adjustments to the basal transcription rate of *per*.

3 Analyzing Coupled *Drosophila melanogaster* Neurons

As demonstrated above, single cell simulation can be used to tune the simulation of a population, bringing about the desired synchrony. In this section, we present single cell analysis as a complement to simulation and demonstrate that it yields a better understanding of the behavior of a coupled population. We analyze the phase behavior of an SDE model of 100 coupled neurons of the *Drosophila melanogaster* circadian pacemaker. In an investigation of potential coupling mechanisms, Ueda *et al.* [12] developed a framework with 960 potential coupling mechanisms, each of which includes a component that sends a signal to neighboring cells. This signal then modulates a given target parameter. The authors show that a subset of the signal/target pairs produce spontaneous (phase) synchronization among the cells. We expand upon their analyses by modeling all 960 signal/target pairs, 84 of which produce (phase) synchrony. However, not all synchronizing mechanisms produce the same behavior. Notably, the period of oscillation is different for each pair and ranges between 20-37 hours. Because we are interested in rhythms that are circadian, we simulate the 82 pairs that produce periods within 20-28 hours. The data describe *what* will happen, but leave unanswered questions such as: *Why* are some signal/target pairs



(a) *Per* mRNA in the Coupled 3×3 Grid



(b) Order Parameter Radius for the 3×3 Coupled Grid

Figure 2: (a) The time series of *per* mRNA concentration is shown for a single SSA simulation of a 3×3 grid of cells uncoupled for the first 24 hours, coupled thereafter. The boundary effects of the small grid size cause differences in amplitudes. (b) For 25 SSA simulations of the grid, we show the mean degree of phase coherence with error bars indicating the standard deviation.

speeding up the oscillations and some slowing them down? *How* would an adjustment of the relative timing between the signal and the cell's phase change the timing?

3.1 Theoretical Background

To study the effects of signaling on the phase behavior, we must examine the effects of parametric manipulation on phase behavior. Thus we use the parametric impulse phase response curve (pIPRC) [24], which predicts the oscillator's velocity change in response to parametric perturbation. To use the pIPRC, we are compelled to investigate a deterministic model. Thus we study a single neuron, modeled as a set of ODEs with a stable attracting limit cycle, $\dot{\mathbf{x}}(t) = \mathbf{f}(\mathbf{x}(t), \mathbf{p})$. The solution along the limit cycle is periodic with period τ , and we describe its progress along the cycle by its phase, ϕ . When the clock is unperturbed, the phase progresses at the same rate as time, $d\phi(\mathbf{x}(t), \mathbf{p})/dt \equiv 1$. When the clock is perturbed, the velocity response is predicted by the pIPRC:

$$\mathbf{pIPRC}(\phi) = \frac{d}{d\mathbf{p}} \frac{d\phi}{dt}(t).$$

Computation is relatively straight forward, requiring only the solution of the adjoint linear variational equation and the differentiation of \mathbf{f} with respect to \mathbf{p} [24]. Interpretation is also straight forward. Consider a signal $\Delta p_j(t, \phi)$ which is a function of either time or phase. This signal will change the oscillator’s velocity according to $\Delta\phi/\Delta t \approx \text{pIPRC}_j(\phi)\Delta p_j(t, \phi)$. Another interpretation is that for a pulse of duration Δt , a phase shift is incurred according to $\Delta\phi \approx \text{pIPRC}_j(\phi)\Delta p_j(t, \phi)\Delta t$. Using this interpretation, the pIPRC predicts the PRC: the pIPRC characterizes the timing behavior of an oscillator alone, while the PRC describes the response to a particular signal.

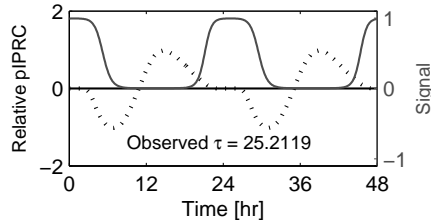
3.2 Methodology

To understand the period of the synchronized cells of the *Drosophila* clock, we study the relationship between the signal and the pIPRC for the target. To acquire the signal, we capitalize on the stable synchrony – in a synchronized system, each neuron sends the same signal at the same time. Thus, we mimic the intercellular signaling simply by assuming that all signals match that of a *single* neuron. The trace of the signal is acquired by simulating one cell as it sends the signal (without allowing the signal to feed back onto the cell). Using this method, the signal and pIPRCs share the same period and can be plotted together for ease of comparison. Two example signals along with the pIPRCs corresponding to their targets are shown in Fig. 3.

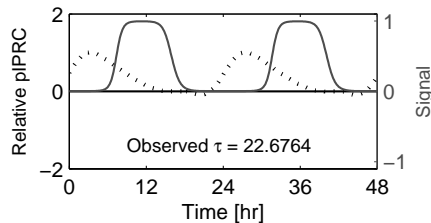
Before we begin our analysis, we evaluate the predictive power of the single cell model and of the pIPRC for each signal/target pair. First, we predict the period of the synchronized SDE population by simulating the ODE model, allowing it to signal itself. After several cycles it converges to a new limit cycle with a new period – the period of the synchronized system. In Fig. 4 we plot our prediction for the new period against the observed period of the SDE model of the full population. The square of the Pearson correlation coefficient, R^2 , is 0.91 and the data is located within an hour of the observed values. Second, we use the pIPRC directly to make similar predictions. By treating ϕ as the independent variable (instead of time), we predict the change in period by assessing the effect of the signal on the oscillator over a single cycle. Integrating over the cycle,

$$\Delta\tau \approx - \int_0^\tau \text{pIPRC}_j(\phi)\Delta p_j(\phi) d\phi,$$

we find that the predictions are qualitatively accurate. Fig. 4 shows the predicted period change of the synchronized system versus the observed period change of the synchronized system. The R^2 value between observed and predicted periods is 0.65. The data are more scattered than those from the full cell simulation, though the majority are within 1 hour of perfect prediction. We conclude that although neither of these



(a) Signal/Target Pair Producing Slow Oscillations



(b) Signal/Target Pair Producing Fast Oscillations

Figure 3: The pIPRC (black dotted line) and signal trace (gray solid line) pairs cause the coupled SDE system to synchronize with (a) long and (b) short periods. All curves are relative to the target parameter's nominal value.

methods are perfect predictors, their qualitative correctness supports our approach.

3.3 Phase Response Behavior

Fig. 3(a) shows the relationship for a pair that causes the system to slow down. In this case, the target reaction rate is the maximal rate of degradation for clock component *tim* mRNA. The signal arrives at the tail end of the advance zone, and is active during the deadzone and the first half of the delay zone, leading to a cycle that is slower than nominal. Fig. 3(b) shows a pair for which the target reaction rate is the maximal rate of *clk* mRNA degradation. Here, the pIPRC shows nearly negligible delay regions. It follows that, regardless of the phase relationship between the signal and target, the oscillator will respond by speeding up.

In both of these cases (and in all cases that produce synchrony), the relationship between the signal and target meets the criteria for stable entrainment (data not shown). If the signal arrives early (because the phase of the system is a little behind), the system is sped up more (or slowed down less) than usual, and vice versa. The study of the pIPRC and signal is consistent with the observed behavior – the mutual entrainment is stable and the system remains synchronized. However,

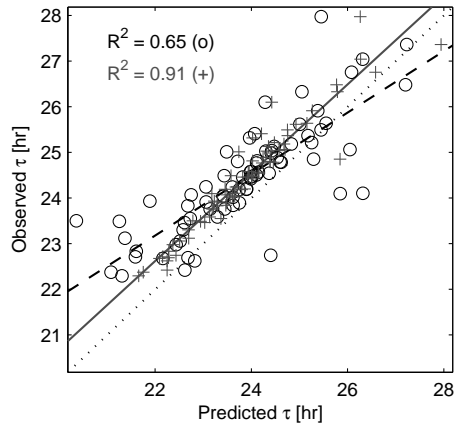


Figure 4: Observed vs. Predicted Periods. For each signal/target pair that produces synchrony there is a black circle and a gray plus. The x-axis position indicates the period predicted using the pIPRC (circles) or using a single cell, signaling itself (pluses). For both data, the y-axis position indicates the period observed once collection of noisy cells becomes (and remains) synchronized. Perfect predictions fall on the dotted line. The dashed and solid lines represent the best fit by linear regression analysis, with $R^2 = 0.65$ for the pIPRC-predicted data and $R^2 = 0.91$ for the single-cell data.

meeting the conditions for mutual entrainment is merely a *necessary* factor; there exist pairs that meet the requirements for stable entrainment but do not yield a transition to synchrony (data not shown). In Fig. 3(a), a leftward signal shift of several hours produces a greater overlap of the advance region, meets the conditions for stable entrainment, and shortens the synchronized period. Thus, an understanding of the phase response behavior is key to unraveling the mechanisms *in vivo*.

4 Phase Entrainment

Just as signaling among cells serves to synchronize the phase of the network, signals from the environment serve to entrain, or reset, the phase of emergent coherent oscillators. More specifically, environmental factors such as light induce phase shifts that calibrate an organism’s internal phase to external time.

Exploring phase resetting through controlled light pulses is not a recent interest. In the early 1970’s, Daan and Pittendrigh investigated light-induced phase shifts in free-running organisms through the development of phase response curves. Watanabe *et al.* [25] built upon Daan and Pittendrigh’s investigation of light-induced phase shifts in free-running organisms by proving that entrainment in mammals involves both advance and delay components of the phase response curve. Boulos *et al.* [6] extended the application of phase response curves by establishing bright light treatment as a means to accelerate circadian re-synchronization rates. Similarly, Forger *et al.* [26] invoke calculus of variations and an analysis of phase space to find the optimum stimuli that start, stop, and reset the phase of a simplified biological oscillator. In a previous study, we optimized the re-synchrony of a detailed mammalian circadian oscillator to the environment through the systematic application of light. We showed that a closed-loop model predictive control (MPC) algorithm is an effective (and realistic) means of resetting the organisms’ phase [27]. Through MPC, we were able to minimize the phase difference between the organism (modeled as a single deterministic oscillator) and the environment. Here, we investigate phase resetting dynamics as a function of the MPC tuning parameters (described in section 4.2) as well as the attributes of the driving force (light).

4.1 A General Nonlinear Mammalian Model

The circadian dynamics of a single deterministic *Mus musculus* limit cycle oscillator [9] serves as the example system. The model is generalized as a set of nonlinear ordinary differential equations with time t , n -length state vector $\mathbf{x}(t)$, environmental light input $L(t)$, controlled light input $u(t)$, and system dynamics $\mathbf{f}(\mathbf{x}(t), L(t), u(t))$:

$$\begin{aligned}\dot{\mathbf{x}}(t) &= \mathbf{f}(\mathbf{x}(t), L(t), u(t)), \\ \mathbf{x}(t_0) &= \mathbf{x}(0).\end{aligned}$$

In this paper the nominal model (a version of the model that has converged to the natural light/dark environment where $u(t) = 0$ and $L(t)$ oscillates as a square wave between values 3.39×10^{-2} and 0) is used to define the reference, $\mathbf{r}(t)$. A circadian time of 0 reflects dawn while a circadian time of 12 reflects dusk, assuming regular 24 hour day/night cycles.

4.2 Optimizing the Manipulated Control Profile

Model predictive control [28] is used to increase the resynchronization rate of circadian oscillators through the systematic addition of light. The algorithm follows a sample and hold strategy, updating the prediction and control input every $t_s = 2\text{hr}$, where the discrete time index $k = t|_{t_s}$. The manipulated light profile, $u(k)$, optimizes an open-loop performance objective on a time interval extending from the current time to the current time plus a prediction horizon, $P = 54\text{hr}$, allowing the algorithm to take control action at the current time in response to a forecasted error. The move horizon, M , limits the number of controlled light pulses within the prediction horizon. Beyond M hours of simulation, the predicted model defaults to $u(k) = 0$. Future behaviors for a variety of control inputs are computed according to the model of the plant.

Given $u_{min} = -3.39 \times 10^{-2}$, $u_{max} = 3.39 \times 10^{-2}$, and $L(k) + u(k) \geq 0$, the cost function penalizes the normalized predicted error between the reference and controlled trajectories, $\mathbf{e}(k)$, and its corresponding control sequence, $\mathbf{u}(k)$. To avoid penalizing transient effects, the state error is weighted uniformly over the move horizon and with increasing weight of slope 2 over the prediction horizon (via \mathbf{Q}). The cost of applying a light input is always weighted uniformly (via \mathbf{R}).

The performance of an M -length control input is measured by

$$J = \min_{\mathbf{u}(\cdot)} \left[(\mathbf{e}\mathbf{Q})^T (\mathbf{e}\mathbf{Q}) + (\bar{\mathbf{u}}\mathbf{R})^T (\bar{\mathbf{u}}\mathbf{R}) \right].$$

Only the first move of the lowest cost control sequence, \mathbf{u}^* , is implemented. Feedback is incorporated by using the next measurement to update the optimization problem. Once the controlled state trajectories converge to within 15% of the reference state trajectories, the system is considered to have recovered its phase in $T_r = \min_k [|e(k)|_\infty \leq 0.15]$ hours. For further details, the reader is referred to [27].

4.3 Tuning the MPC Parameters

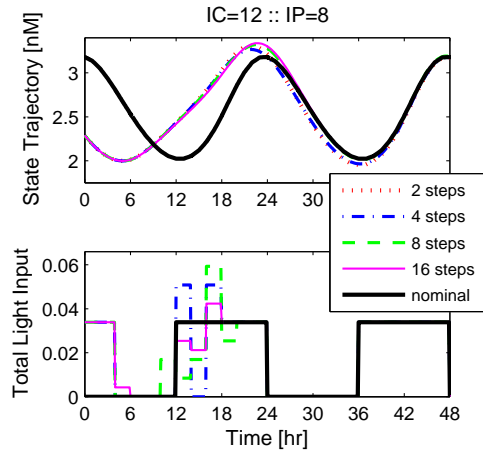
The best fit control sequence is determined by enumerating the solutions over a grid in the solution space (light magnitude as a function of time). The algorithm approaches a globally optimal solution as the total possible quantization steps of the control input increases. We test the efficacy of the algorithm with respect to a quantization of 2, 4, 8, and 16 steps. Results suggest that the shorter recovery time may not outweigh the increase in computation time (Fig. 5(a)). Therefore, we investigate solutions for 2 and 8 possible control values.

Similarly, we evaluate the algorithm with respect to a control input of duration 1, 2, and 3 hours (reflecting a move horizon of 3, 6, and 9-hours, respectively). Although shorter light pulses offer a more dynamic manipulated variable profile, it shortens the move horizon and may reduce the utility of model predictive control (Fig. 5(b)). Conversely, a longer pulse may reduce the possible control profiles since extended exposure to light leads to arrhythmic behavior [29]. We set the duration of control to 2 hours.

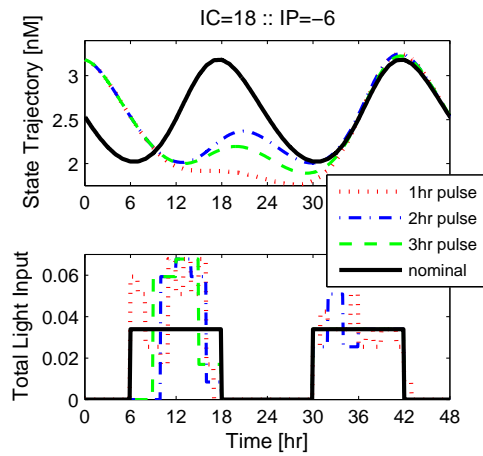
4.4 Phase Recovery Dynamics

The nonlinear properties of biological oscillators often cause different phase-resetting times with respect to the initial condition (IC, the circadian time at which the control begins), and initial phase difference (IP, the amount of circadian time that needs to be recovered). We generate phase recovery dynamics for the open-loop algorithm where environmental light/dark cycles entrain the system (Fig. 4.4), and the closed-loop MPC algorithm where the manipulated control variable (light) has 2 and 8 possible values (Fig. 7). Since nonlinearity also challenges the uniqueness of optimal light sequences, we choose the control profile that minimizes the magnitude of total admitted light, hence penalizing the weighted sum of $\mathbf{u}(\cdot)$ (refer to section 4.2).

Recovery times are described as a function of both the initial condition and initial phase difference to better visualize the nonlinear dynamic behavior of phase resetting. The open-loop environmental control strategy (Fig. 4.4) requires (at most) 64.7 hours to synchronize a ± 12 -hour initial phase difference beginning at an initial condition of 12-hours (Table 1) [27]. The closed-loop 2-step algorithm (Fig. 7(a)) improves upon the maximum recovery time as it requires only 36.8 hours to recover a -6-hour initial phase difference (at IC=18hr). Surprisingly, the 8-step algorithm (Fig. 7(b)) does not significantly improve phase resetting as it requires 34.7 hours to recover the same conditions. For this reason, a 2-step algorithm (which requires approximately 0.17hr of computation time per simulation) is more efficient for real-world applications – such as light therapy – when compared to the 8-step algorithm (which requires approximately 3.5hr of computation time per simulation).



(a) Quantization of Light Profiles



(b) Duration of Controlled Light Pulses

Figure 5: Top subplots depict state dynamics as they converge to the reference trajectory, the bold solid lines. Lower subplots depict the light profiles used to reset the phase differences; these sequences also converge to nominal light/dark cycles, the bold solid lines. Control action begins at (a) 12 hours and (b) 18 hours, resetting phase differences of (a) 8 hours and (b) -6 hours. The recovery time associated with a control input that allows 2, 4, 8, and 16 possible values (a) is 36.8, 35.6, 34.7, and 34.6-hours respectively. The recovery time associated with a 1, 2, and 3-hour control input (b) is 36.7, 34.7, and 35.2-hours respectively.

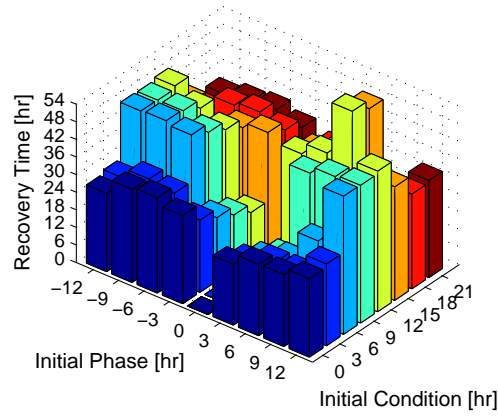
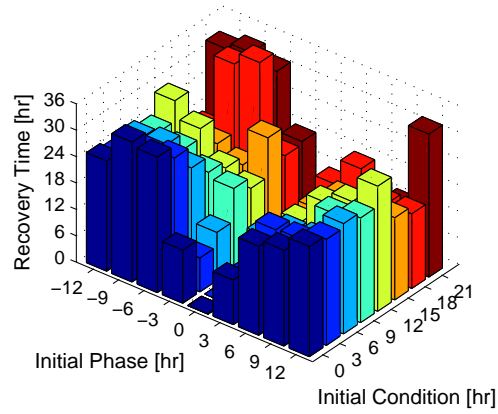


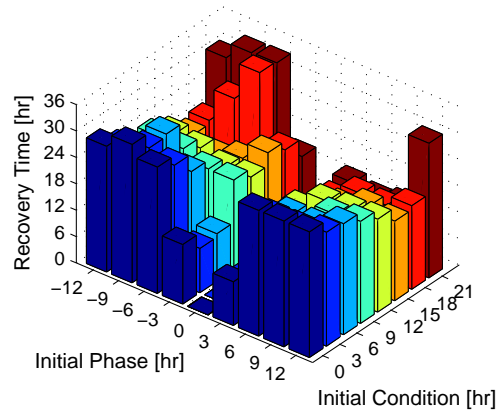
Figure 6: The open-loop (natural) phase recovery dynamics as a function of the initial condition and initial phase difference. The shading of recovery times (shown on the vertical axis) is consistent along the initial condition and among the figures 7(a) and 7(b).

Table 1: Maximum recovery times (in hours) with respect to initial conditions and initial phase differences (also in hours). The bold-face text reflects the maximum recovery time over the entire set.

IC	Open-Loop		2-Step Algorithm		8-Step Algorithm	
	Recovery	IP	Recovery	IP	Recovery	IP
0	32.50	-6	31.80	-9	31.40	-9
3	31.40	-9	28.00	-6	28.10	-9
6	47.50	-9	26.00	-9	28.60	-9
9	46.90	± 12	23.80	± 12	23.20	± 12
12	64.70	± 12	28.40	± 12	21.10	± 12
15	61.70	± 12	24.70	-3	21.50	-3
18	40.80	6	36.80	-6	34.70	-6
21	35.50	-6	34.00	-9	34.30	-6



(a) 2-Step Closed-Loop Control



(b) 8-Step Closed-Loop Control

Figure 7: The shading of closed-loop MPC recovery times (shown on the vertical axis) as a function of the initial condition and initial phase difference is consistent along the initial condition. The vertical axes, however, are not the same; refer to table 1 for a direct comparison of phase resetting dynamics among the presented algorithms. An IC=12hr is one of the few data sets whose recovery time decreases with greater control flexibility.

Although the closed-loop algorithm significantly increases re-synchronization rates, using 2 possible control values is often just as effective as using 8; the flexibility of control has little effect on the MPC algorithm. Such results support the hypothesis that, in general, natural light/dark cycles are not optimized to reset large phase differences [27]. Instead, organisms may have evolved to efficiently reset small phase differences since rapid transit across multiple time zones is a recent innovation. Such results support our use of controlled light pulses to increase re-synchronization rates and alleviate many circadian related disorders [30, 31].

Further studies may include the investigation of phase resetting dynamics as a function of environmental day-length. This application would address circadian-related disorders common among people that live near either pole. As the day-length decreases, people are exposed to less light and may be at a higher risk of de-synchronizing their internal clocks with that of their environment [30, 31].

5 Conclusion

We employ systems theoretic tools to investigate circadian phase properties of single deterministic, and populations of stochastic models. The study of synchronization supports the reverse-engineering of the clock in the SCN while providing a foundation upon which to engineer other communication networks. Analysis of the pIPRC provides separation of the timing characteristics of the oscillator and signal. Altering the signal (duration, magnitude, or shape) can have profound effects prescribed by the pIPRC. For example, it is possible to speed up an oscillator when (and only when) there is an advance area in the target pIPRC. To synchronize, the signal must meet the conditions for stable entrainment. Through model predictive control, we solve for a sequence of light pulses that resets the circadian clock in a fraction of the time required by natural open-loop entrainment. The study of circadian phase dynamics provides a forum to address re-synchronization properties of the clock.

6 Acknowledgements

This project was supported in part by the ICB grant DAAD19-03-D-0004; NIH grant GM078993; NSF IGERT grant DGE02-21715; NIH grant EB007511; Army Research Office grant W911NF-07-1-0279; and The Research Participation Program between the US DOE and AFRL/HEP.

References

- [1] Kitano, H.: ‘Systems biology: a brief overview,’ *Science*, 2002, **295**, pp. 1662–1664
- [2] Fall, C.P., Marland, E.S., Wagner, J.M. and Tyson, J.J.: *Computational Cell Biology*. (Springer, New York, 2005)
- [3] Reppert, S.M. and Weaver, D.R.: ‘Coordination of circadian timing in mammals’, *Nature*, 2002, **418**, pp. 935–941
- [4] Herzog, E.D., Aton, S.J., Numano, R., Sakaki, Y., and Tei, H.: ‘Temporal precision in the mammalian circadian system: a reliable clock from less reliable neurons’, *J. Biol. Rhythm.*, 2004, **19**, pp. 35–46
- [5] Liu, A.C., Welsh, D.K., Ko, C.H., Tran, H.G., Zhang, E.E., Priest, A.A., Buhr, E.D., Singer, O., Meeker, K., Verma, I.M., Doyle III, F.J., Takahashi, J.S., and Kay, S.A.: ‘Intercellular coupling confers robustness against mutations in the SCN circadian clock network’, *Cell*, 2007, **129**, pp. 605–616
- [6] Boulos, Z., Macchi, M.M., Stürchler, M.P., Stewart, K.T., Brainard, G.C., Suhner, A., Wallace, G., and Steffen, R. ‘Light visor treatment for jet lag after westward travel across six time zones’, *Aviat. Space Environ. Med.*, 2002, **73**, pp. 953–963
- [7] Dunlap, J.C., Loros, J.J., and DeCoursey, P.J. (Eds.): *Chronobiology: Biological Timekeeping* (Sinauer Associates, Inc., Sunderland, MA, 2004)
- [8] Daan, S., and Pittendrigh, C.S.: ‘A functional analysis of circadian pacemakers in nocturnal rodents. II. The variability of phase response curves’, *J. Comp. Physiol.*, 1976, **106**, pp. 253–266
- [9] Forger, D.B. and Peskin, C.S.: ‘A detailed predictive model of the mammalian circadian clock’, *Proc. Natl. Acad. Sci. USA*, 2003, **100**, pp. 14806–14811
- [10] Leloup, J.-C., and Goldbeter, A.: ‘Toward a detailed computational model for the mammalian circadian clock’, *Proc. Natl. Acad. Sci. USA*, 2003, **100**, pp. 7051–7056
- [11] Geier, F., Becker-Weimann, S., Kramer, A., and Herzog, H.: ‘Entrainment in a model of the mammalian circadian oscillator’, *J. Biol. Rhythm.*, 2005, **20**, pp. 83–93
- [12] Ueda, H.R., Hirose, K., and Iino, M.: ‘Intercellular coupling mechanism for synchronized and noise-resistant circadian oscillators’, *J. Theor. Biol.*, 2002, **216**, pp. 501–512

- [13] Gonze, D., and Goldbeter, A.: ‘Circadian rhythms and molecular noise’, *Chaos*, 2006, **16**, no. 026110
- [14] Gonze, D., Bernard, S., Waltermann, C., Kramer, A., and Herzog, H.: ‘Spontaneous synchronization of coupled circadian oscillators’, *Biophys. J.*, 2005, **89**, pp. 120–129
- [15] To, T.-L., Henson, M.A., Herzog, E.D., and Doyle III, F.J.: ‘A molecular model for intercellular synchronization in the mammalian circadian clock’, *Biophys. J.*, 2007, **92**, pp. 3792–3803
- [16] Aton, S.J., Colwell, C.S., Harmar, A.J., Waschek, J., and Herzog, E.D.: ‘Vasoactive intestinal polypeptide mediates circadian rhythmicity and synchrony in mammalian clock neurons’, *Nat. Neurosci.*, 2005, **8**, pp. 476–483
- [17] Piggins, H.D., Antle, M.C., and Rusak, B.: ‘Neuropeptides phase shift the mammalian circadian pacemaker’, *J. Neurosci.*, 1995, **15**, pp. 5612–5622
- [18] Hao, H., Zak, D.E., Sauter, T., Schwaber, J., and Ogunnaike, B.A.: ‘Modeling the VPAC2-activated cAMP/PKA signaling pathway: from receptor to circadian clock gene induction’, *Biophys. J.*, 2006, **90**, pp. 1560–1571
- [19] Gillespie, D.T.: ‘The chemical langevin equation’, *J. Chem. Phys.*, 2000, **113**, pp. 297–306
- [20] StochKit, 2007, <http://www.cs.ucsb.edu/~cse/StochKit>
- [21] Gillespie, D.T.: ‘A general method for numerically simulating the stochastic time evolution of coupled chemical reactions’, *J. Comput. Phys.*, 1976, **22**, pp. 403–434
- [22] —, ‘Exact stochastic simulation of coupled chemical reactions’, *J. Phys. Chem.*, 1977, **81**, pp. 2340–2361
- [23] Strogatz, S.H.: ‘From Kuramoto to Crawford: exploring the onset of synchronization in populations of coupled oscillators’, *Physica D*, 2000, **143**, pp. 1–20
- [24] Taylor, S.R., Gunawan, R., Petzold, L.R., and Doyle III, F.J.: ‘Sensitivity measures for oscillating systems: Application to mammalian circadian gene network’, *IEEE Trans. Circuits Syst. I*, 2007, submitted
- [25] Watanabe, K., Deboer, T., and Meijer, J.H.: ‘Light-induced resetting of the circadian pacemaker: Quantitative analysis of transient versus steady-state phase shifts’, *J. Biol. Rhythm.*, 2001, **16**, pp. 564–573

- [26] Forger, D.B., and Paydarfar, D.: ‘Starting, stopping, and resetting biological oscillators: in search of optimum perturbations’, *J. Theor. Biol.*, 2004, **230**, pp. 521–532
- [27] Bagheri, N., Stelling, J. and Doyle III, F.J.: ‘Circadian phase entrainment via nonlinear model predictive control’, *Int. J. Robust Nonlinear Control*, 2007, published on-line
- [28] Morari, M. and Lee, J.H.: ‘Model predictive control: Past, present and future’, *Comput. Chem. Eng.*, 1999, **23**, pp. 667–682
- [29] Ohta, H., Yamazaki, S., and McMahon, D.G.: ‘Constant light desynchronizes mammalian clock neurons’, *Nat. Neurosci.*, 2005, **8**, pp. 267–269
- [30] Lamberg, L.: *Bodyrhythms: chronobiology and peak performance* (William Morrow and Company, INC., New York, NY, 1994)
- [31] Moore, R.Y.: ‘Circadian rhythms: Basic neurobiology and clinical applications’, *Annu. Rev. Med.*, 1997, **48**, pp. 253–266